Published OnlineFirst October 20, 2011; DOI: 10.1158/1078-0432.CCR-11-1536

Cancer Therapy: Preclinical

Clinical Cancer Research

Characterization of Alisertib (MLN8237), an Investigational Small-Molecule Inhibitor of Aurora A Kinase Using Novel *In Vivo* Pharmacodynamic Assays

Mark G. Manfredi, Jeffrey A. Ecsedy, Arijit Chakravarty, Lee Silverman, Mengkun Zhang, Kara M. Hoar, Stephen G. Stroud, Wei Chen, Vaishali Shinde, Jessica J. Huck, Deborah R. Wysong, David A. Janowick, Marc L. Hyer, Patrick J. LeRoy, Rachel E. Gershman, Matthew D. Silva, Melissa S. Germanos, Joseph B. Bolen, Christopher F. Claiborne, and Todd B. Sells

Abstract

Purpose: Small-molecule inhibitors of Aurora A (AAK) and B (ABK) kinases, which play important roles in mitosis, are currently being pursued in oncology clinical trials. We developed three novel assays to quantitatively measure biomarkers of AAK inhibition *in vivo*. Here, we describe preclinical characterization of alisertib (MLN8237), a selective AAK inhibitor, incorporating these novel pharmacodynamic assays.

Experimental Design: We investigated the selectivity of alisertib for AAK and ABK and studied the antitumor and antiproliferative activity of alisertib *in vitro* and *in vivo*. Novel assays were used to assess chromosome alignment and mitotic spindle bipolarity in human tumor xenografts using immunofluorescent detection of DNA and alpha-tubulin, respectively. In addition, 18F-3′-fluoro-3′-deoxy-L-thymidine positron emission tomography (FLT-PET) was used to noninvasively measure effects of alisertib on *in vivo* tumor cell proliferation.

Results: Alisertib inhibited AAK over ABK with a selectivity of more than 200-fold in cells and produced a dose-dependent decrease in bipolar and aligned chromosomes in the HCT-116 xenograft model, a phenotype consistent with AAK inhibition. Alisertib inhibited proliferation of human tumor cell lines *in vitro* and produced tumor growth inhibition in solid tumor xenograft models and regressions in *in vivo* lymphoma models. In addition, a dose of alisertib that caused tumor stasis, as measured by volume, resulted in a decrease in FLT uptake, suggesting that noninvasive imaging could provide value over traditional measurements of response.

Conclusions: Alisertib is a selective and potent inhibitor of AAK. The novel methods of measuring Aurora A pathway inhibition and application of tumor imaging described here may be valuable for clinical evaluation of small-molecule inhibitors. *Clin Cancer Res; 17(24); 7614–24. ©2011 AACR.*

Introduction

Mitotic kinases, kinesins, and other mitotic enzymes are being pursued as targets for the next generation of antimitotic therapies in oncology. Although several molecules have shown clinical efficacy, it is too early to know whether they will add benefit beyond classic microtubule antagonists such as the taxanes and vinca alkaloids. So far, however, it is clear that the newer agents are unlikely to cause the peripheral neuropathy, often observed in patients treated with microtubule-targeting drugs (1).

The conventional view of antimitotic agents is that they cause prolonged mitotic arrest leading to cell death. In recent years, this perspective has been modified to incorporate 2 alternative outcomes following mitotic delays in metaphase (2, 3). Studies using live-cell microscopy with a variety of antimitotic agents in a range of cell lines have reported a striking diversity of responses (4–6). In some sensitive cell lines, mitotic arrest is sustained until cells die directly from prometaphase. In other sensitive cell lines, the mitotic delay is transient, and it is followed by an inappropriate segregation of unaligned chromosomes (4, 5, 7). This mitotic slippage is followed by a variety of terminal outcomes that seem to include postmitotic death as well as terminal growth arrest (cellular senescence; refs. 8, 9). Evidence exists to support the view that cytostasis (10, 11) as well as postmitotic cell death (5) are significant drivers of the antiproliferative effects of taxanes.

Authors' Affiliation: Millennium Pharmaceuticals, Inc., Cambridge, Massachusetts

Note: Supplementary data for this article are available at Clinical Cancer Research Online (http://clincancerres.aacrjournals.org/).

Corresponding Author: Mark G. Manfredi, Millennium Pharmaceuticals, Inc., Cambridge, 40 Landsdowne Street, Cambridge, MA 02139. Phone: 617-679-7382; Fax: 617-551-8906; E-mail: mark.manfredi@mpi.com

doi: 10.1158/1078-0432.CCR-11-1536

Published OnlineFirst October 20, 2011; DOI: 10.1158/1078-0432.CCR-11-1536

Translational Relevance

Aurora A kinase (AAK) has been implicated in oncogenesis and tumor progression and is amplified or overexpressed in several tumor types. In this article, we describe the development of 3 novel biomarker assays of AAK activity that provide detailed and specific information with regard to the biological effects of AAK inhibition *in vivo*. The novel assays, therefore, provide a basis for translating the mechanism of action of AAK inhibitors into clinically informative pharmacodynamic endpoints. In conjunction with established methods, these assays were used to describe the *in vitro* and *in vivo* antitumor activity of an investigational AAK inhibitor, alisertib (MLN8237). Our data indicate that alisertib is a selective and potent inhibitor of AAK and supports its continued clinical development as an anticancer agent. Furthermore, the assays described here are currently being deployed in phase I studies to help characterize the activity of alisertib in patients.

The complex mechanism of action of antimitotic agents has posed a significant challenge for the development of pharmacodynamic biomarkers for their action. The obvious and traditional biomarker, the mitotic index, is hampered by the cell line-to-cell line differences in the duration of mitotic arrest (4, 5) and by the tendency of low concentrations of antimitotic agents to reduce cellular viability without a prolonged mitotic arrest, via a mitotic slippage-based mechanism (12, 13). Surprisingly, even within the same cell type, there is often a diversity of responses to the same mitotic inhibitor at different concentrations (4, 5, 13) and heterogeneity in the degree of mitotic arrest versus mitotic slippage within the same population of cells (4, 5). Consistent with these findings, the length of mitotic arrest within a given cell type has been found not to correlate with probability of death (4, 5).

This weak linkage between mitotic arrest and cell death provides us with a retrospective explanation for the failure of early attempts to use the mitotic index to provide guidance for taxane development. For these agents, preclinical *in vivo* work showed minimal (14) or nonexistent (15) predictive value for mitotic index with respect to anticipating the degree of tumor growth inhibition, which was later corroborated in patient tumor biopsies (16).

Aurora A and Aurora B are related serine/threonine kinases that share significant sequence similarity but differ in their localization, substrate specificity, and function. The function of these kinases has been reviewed extensively (17–19); among other functions, Aurora A is essential for normal mitotic spindle formation and centrosome maturation and separation (20). Several Aurora kinase inhibitors are currently undergoing clinical development. These include molecules that are Aurora A selective, Aurora B selective, dual Aurora A and Aurora B inhibitors, and multikinase inhibitors, which include activity against the Aurora kinases (21, 22). Early results from clinical trials of alisertib (MLN8237) and other Aurora kinase inhibitors have shown promising antitumor activity and prolonged stable disease (23–27).

Although inhibition of Aurora kinases can alter the microtubule network (7), a potentially unique feature that may distinguish Aurora kinase inhibitors from the microtubule antagonists as anticancer agents is the additional regulatory functions the Aurora kinases play. For example, Aurora A directly binds to and regulates the turnover of N-myc and may be essential in N-myc amplified neuroblastomas (28). In addition, both Aurora A and Aurora B have been shown to phosphorylate and regulate p53 function in experimental systems (29, 30). Determining which of these additional functions are most important for tumor survival should provide insights into patient stratification strategies or rational combination approaches.

Inhibition of Aurora A kinase (AAK) leads to the formation of mitotic spindle defects and misaligned chromosomes (7, 31, 32). However, despite these mitotic defects, cells lacking functional Aurora A often divide, albeit abnormally (7, 33). This inappropriate division in the presence of spindle defects seems to be the result of compromised spindle assembly checkpoint function (34). The abnormal mitotic divisions result in deleterious aneuploidy and chromosomal instability leading to cell death or arrest (7). However, a portion of cells can recover from these outcomes and can reenter the cell cycle. The alternative fates subsequent to postmitotic defects induced by AAK and Aurora B kinase (ABK) inhibition are mediated in part by the p53 and p73 signaling pathways (35, 36). In addition, Aurora A inhibition in a range of cell types has been shown to lead to a reduction in the rate of mitotic entry because of a late G_2 block in the cell cycle (37–40). As is the case for traditional antimitotic agents, this complexity in the downstream cell biological consequences of Aurora A inhibition has led to challenges in the use of the mitotic index as a pharmcodynamic measurement in tumors. In particular, we have previously shown that the mitotic index is an early marker of Aurora A inhibition (32), which decays gradually over time due to a loss of the cycling population of cells.

To address these limitations in the use of mitotic index in drug development, we developed 3 novel assays to quantitatively measure biomarkers of Aurora A inhibition *in vivo*. The first 2 assays, as reported initially in Chakravarty and colleagues (41), assess chromosome alignment and spindle bipolarity, whereas the final utilizes 18F-3′-fluoro-3′-deoxy-L-thymidine positron emission tomography (FLT-PET) to noninvasively measure tumor cell proliferation. Taken together, the assessed biomarkers provide a more complete view of the biological effects of Aurora A inhibition *in vivo* and have provided a basis for translation of mechanism of action into clinically informative pharmacodynamic endpoints. In this article, we detail these novel methods for quantifying Aurora A inhibition *in vivo*, and using these and other established methods, describe the *in vitro* and *in vivo* antitumor activity of alisertib against AAK. The phenotypic

Published OnlineFirst October 20, 2011; DOI: 10.1158/1078-0432.CCR-11-1536

biomarkers are now being used to analyze tumor biopsies in clinical studies (41), whereas the functional imaging approaches have been used to monitor alisertib activity.

Material and Methods

Enzyme and cell-based assays to measure kinase inhibition

Aurora A and Aurora B radioactive Flashplate enzyme assays and cell-based assays were conducted to determine the nature and degree of alisertib-mediated inhibition *in vitro*, as described by Manfredi and colleagues (32). In the cell-based assays, Aurora A activity was determined by measuring autophosphorylation of Aurora A on threonine 288, whereas Aurora B activity was determined by measuring phosphorylation of histone H3 on serine 10 (pHisH3), in both cases, using high content imaging assays and as previously described (32). The inhibitory activity of 1 μmol/L alisertib was also tested against 205 kinases (SelectScreen kinase panel; Invitrogen).

Flow cytometry

HCT-116 colorectal carcinoma cells (American Type Culture Collection) were plated on 6-well dishes (2×10^5 per well) and propagated in McCoy's 5A media (Gibco) supplemented with 10% FBS. After 18 hours, alisertib at a final concentration of 0.050, 0.250, or 1.000 μmol/L was added, and the cells were grown for an additional 24 hours. Cells treated with dimethyl sulfoxide (DMSO; 0.2%) served as the untreated vehicle control. The cells were harvested with trypsin EDTA 1× (Gibco), washed once with PBS, fixed in 70% ethanol, and stored at 4°C for 1 hour. The cells were resuspended in propidium iodide (1:40; Molecular Probes) and RNAse A (1:5,000; Sigma) in PBS for 30 minutes at 4°C. Cell-cycle distributions were determined by measuring DNA content using flow cytometry (FACS Calibur; Becton Dickenson), and samples were analyzed using Winlist 5.0 software (Verity Topsham).

Immunofluorescent staining

HCT-116 cells were grown for 24 hours on glass coverslips in McCoy's 5A media supplemented with 10% FBS, and alisertib diluted in DMSO to 0.050, 0.250, and 1.000 μmol/L. Cells treated with DMSO served as the vehicle control. Immunofluorescence staining was done with anti–α-tubulin mouse antibodies (diluted 1:1,000; Sigma) and Hoescht (diluted 1:50,000; Molecular Probes). Images were captured as previously described (32).

BrdU *in vitro* cell proliferation assay

Thirteen tumor cell lines treated with increasing concentrations of alisertib over 96 hours were subjected to 5-bromo-2-deoxyuridine (BrdU) incorporation as a measurement of cellular proliferation. Proliferation of each cell line was measured using the cell proliferation ELISA, BrdU colorimetric kit according to the manufacturer's recommendations (Roche), and as previously described (32).

In vivo efficacy studies

Nine *in vivo* tumor models of different histologies grown subcutaneously or disseminated were developed in either nude or severe combined immunodeficient (SCID) mice (Charles River). The methods for all *in vivo* studies have been described previously (32), with the exception of the lymphoma tumor models described below. All mice had access to food and water *ad libitum* and were housed and handled in accordance with the Guide for the Care and Use of Laboratory Animals and Millennium Institutional Animal Care and Use Committee Guidelines. Mice for all models were dosed orally with alisertib for approximately 3 weeks and tumor growth inhibition (TGI) was calculated on the last day of treatment. For all studies, alisertib was formulated in 10% 2-hydroxypropyl-β-cyclodextrin and 1% sodium bicarbonate and was dosed orally by gavage on a once-daily or twice-daily schedule.

The cell lines OCI-LY7-Luc, OCI-LY19-Luc, and WSU-DLCL2-Luc were used for lymphoma models; tumor cells were inoculated intravenously into 5- to 8-week-old female SCID (nonobese diabetic SCID; Taconic, in study of OCI-LY7-Luc) mice. Mice bearing the disseminated, CD20-positive, non-Hodgkin's lymphoma model OCI-LY19 were treated with vehicle control (10% 2-hydroxypropyl-β-cyclodextrin and 1% sodium bicarbonate was used for all *in vivo* studies), alisertib at 20 mg/kg twice daily or 30 mg/kg once daily, or the anti-CD20 monoclonal antibody rituximab (Rituxan; Genentech) at 10 mg/kg once per week. The lymphoma cell lines stably expressed firefly luciferase, and tumor growth over time was measured using whole-body bioluminescent imaging using Xenogen IVIS 200 imaging system (Caliper). Fifteen minutes before imaging, mice received an intraperitoneal injection of 150 mg/kg of the substrate Luciferin (Caliper), which when oxidized by luciferase emits light photons. Mice were imaged both dorsally and ventrally, and photon flux values were summed from both views. The antitumor effects of each treatment group were determined by calculating the percent TGI [(Δ control mean tumor photon flux − Δ treated mean tumor photon flux) × 100/Δ control mean tumor photon flux] at the end of treatment.

Mitotic index, spindle bipolarity, and chromosome alignment assays

Mice bearing HCT-116 xenografts were treated orally with a single dose of 3, 10, and 30 mg/kg alisertib, and tumor samples were removed at specified time points. Frozen tumor tissue sections were stained for the mitotic marker pHisH3, then visualized using immunofluorescence detection and quantified at the indicated time points. The methods used to stain and quantify pHisH3, which is also an Aurora B substrate, have been described previously (32). Aurora B inhibition would result in a decrease in pHisH3, whereas Aurora A inhibition would result in an increase in the mitotic marker (32). For chromosome alignment and spindle bipolarity assays, tumor samples were harvested from mice bearing HCT-116 xenograft tumors at specified time points, then formalin fixed and paraffin embedded.

Published OnlineFirst October 20, 2011; DOI: 10.1158/1078-0432.CCR-11-1536

The samples were sectioned at 5 μm and stained using the Discovery XT automated slide staining instrument (Ventana Molecular Discovery Systems). Sections were deparaffinized on the instrument with EZ prep solution (Ventana Medical Systems) and antigen retrieval was completed with CC1 (Ventana Medical Systems). Immunofluorescence staining for tubulin was done using a mouse anti–α-tubulin clone DM1A fluorescein isothiocyanate–conjugated antibody (1:100; Sigma) and for DNA using 4′, 6-diamidino-2-phenylindole (DAPI; Vector Laboratories) for 60 minutes. For each mitotic cell, 26 focal planes spaced 0.2 μm apart were acquired using an automated Nikon microscope using 40× objective. To remove out-of-focus light, the image stacks were processed using MetaMorph imaging software (Molecular Devices). Three-dimensional projections of each cell were also generated using MetaMorph imaging software. These projections enable reconstruction of the entire spindle structure across the 5-μm section thickness. The projections were presented in a randomized and blinded fashion to 3 scorers. Each mitotic cell was scored for chromosome alignment (aligned vs. not aligned) and spindle bipolarity (bipolar vs. not bipolar) according to preestablished criteria. Scorers have the option for a "no-call" vote. Scores chosen by the majority of the reviewers was used for subsequent calculations. Spindles and chromosomes for which no majority call existed were discounted from the analysis.

FLT-PET

HCT-116 cells (5×10^6 cells) diluted in 100 μL PBS were inoculated subcutaneously into the right flank of 20 nude mice. When the tumors reached approximately 200 mm^3 by caliper measurement, the animals were randomized into vehicle and treatment groups ($n = 8$ per group) and received alisertib at 20 mg/kg twice daily or vehicle control, respectively, for a period of 21 days. PET imaging was conducted using the proliferation marker FLT, which reflects the activity of thymidine kinase 1 (42). FLT-PET scanning was conducted on days 0 (baseline), 7, 14, and 21 post-alisertib treatment. Approximately 200 μCi (194–236 μCi, 7.2–8.7 MBq) of F^{18}-FLT (PETNET) was injected via tail vein on days 0 (before alisertib treatment), 7, 14, and 21, and allowed to distribute in conscious animals for 60 minutes. Mice were then anesthetized with 2% isoflurane and positioned prone in a custom, 2-animal holder. A 10-minute scan was done using the R4 microPET system (Siemens Medical), followed by a 10-minute attenuation correction scan. Tomographic images were subsequently reconstructed using the 2-dimensional ordered subset expectation maximization method. To minimize the influence of necrotic tissue in the HCT-116 xenograft during image analysis, a 27-mm^3 volume-of-interest (VOI) within a viable region of the tumor was selected using AMIDE software (Molecular Imaging Program at Stanford, Stanford University; ref. 43). The data was analyzed as the standardized uptake value (SUV) of the VOI, SUV_{VOI}, and was normalized to baseline.

Results

In vitro studies show that alisertib inhibits AAK and is selective over family member ABK and other kinases

Alisertib has a benzazepine core structure with a fused amino pyrimidine ring and an aryl carboxylic acid (Supplementary Fig. S1). In enzymatic assays, alisertib was a potent inhibitor of AAK, with an IC_{50} value of 1.2 nmol/L (Table 1). Alisertib has less activity against ABK, with an IC_{50} value of 396.5 nmol/L in enzymatic assay. The cell-based assays showed that alisertib was at least 200-fold more selective for Aurora A ($IC_{50} = 6.7$ nmol/L) than Aurora B ($IC_{50} = 1{,}534$ nmol/L; Supplementary Fig. S2). In addition, alisertib showed selectivity in enzymatic assays against a 205-kinase panel (Supplementary Fig. S3).

Phenotypic cell–based assays supported the selectivity of alisertib for AAK over ABK. At a concentration of 0.050 μmol/L alisertib, cell-cycle analysis using flow cytometry showed an increase in cells in the G_2/M phase at 24 and 48 hours (Fig. 1A), a phenotype consistent with Aurora A inhibition (7, 32). In addition, cells treated at this concentration displayed mitotic spindle abnormalities and chromosome misalignment (Fig. 1B), phenotypes that were previously described to be associated with Aurora A inhibition (7). At higher concentrations of 0.250 and 1.000 μmol/L, alisertib-treated cells showed phenotypes consistent with Aurora B inhibition. At these concentrations, cell-cycle analysis showed an increase in the number of cells with 8N DNA content (Fig. 1A). In addition, immunofluoresent staining of chromosomes and α-tubulin suggested that these cells are multinucleated (Fig. 1B).

Alisertib inhibits proliferation of tumor cells grown in culture from diverse origin

Alisertib displayed antiproliferative activity in a broad panel of adherent and suspended cell lines (Table 2). Alisertib inhibited cell proliferation with IC_{50} values ranging from 15 to 469 nmol/L. In general, lymphoma

Table 1. IC_{50} values of alisertib against recombinant Aurora A and Aurora B as determined by a radioactive Flashplate assay, against Aurora A and Aurora B activity in HeLa cells

	Cell line	Alisertib IC_{50} (nmol/L)
Aurora A	Recombinant Aurora A	1.2
	HeLa	6.7
Aurora B	Recombinant Aurora B	396.5
	HeLa	1,534

Published OnlineFirst October 20, 2011; DOI: 10.1158/1078-0432.CCR-11-1536

Table 2. Inhibition of proliferation by alisertib in tumor cell lines, as assessed by the BrdU cell proliferation assay

	Cell line	Alisertib IC_{50} (nmol/L)
Colon	HCT-116	32 ± 10 (8)[a]
	SW480	431 ± 159 (8)
	DLD-1	469 (1)
Lung	H460	16 (1)
Breast	MDA-MB-231	190 (1)
Prostate	PC3	54 (1)
Ovarian	SKOV3	111 (1)
Pancreatic	HPAC	130 (1)
Lymphoma (DLBCLs)	OCI-LY-3	43 (1)
	OCI-LY-7	86 (1)
	OCI-LY-10	16 (1)
	OCI-LY-19	15 (1)
	WSU	50 (1)

[a]Numbers represent average IC_{50} ± SD derived from the BrdU cell proliferation ELISA assay.
Numbers in parentheses represent the number of experiments completed.

cell lines were more sensitive to alisertib than solid tumor cell lines.

Pharmacodynamic activity of alisertib *in vivo*: increased mitotic index, reduced bipolar mitotic spindles, and increased chromosome alignment abnormalities

Alisertib dosed orally at 3, 10, and 30 mg/kg in female nude mice bearing HCT-116 colon tumor xenografts resulted in significant bioavailability, as measured by plasma and tumor concentrations (Supplementary Fig. S4). A dose of 30 mg/kg on a once daily schedule was the maximum tolerated dose (MTD).

Analysis of tumor tissue from HCT-116 xenografts treated with increasing doses of alisertib revealed a time-dependent and dose-dependent increase in the mitotic marker pHisH3, suggesting that alisertib inhibited Aurora A (Fig. 2A). The plasma concentration at the time the mitotic marker was declining was approximately 1 to 2 μmol/L, suggesting that this concentration is needed to inhibit AAK *in vivo* (Supplementary Fig. S4). Moreover, there was no inhibition of pHisH3 at concentrations of approximately 6 μmol/L showing a significant selectivity for Aurora A inhibition over Aurora B *in vivo*.

To further characterize the *in vivo* phenotype of Aurora A inhibition, tumors treated with alisertib at the doses used above were assessed for chromosome alignment and mitotic spindle defects. To assess mitotic tumor cells for chromosome alignment and spindle bipolarity, sections were stained for α-tubulin and DNA. Representative examples of mitotic cells from each of the time points in the first 4 hours at all 3 dose levels are shown in Fig. 2B and illustrate a broad dose- and time-dependent decrease in the degree of chromosome alignment and spindle bipolarity during mitosis, consistent with the described mechanism of Aurora A. As the figure shows, mitotic spindles in the control sample showed a high degree of chromosome alignment and bipolarity. Figure 2C and D show that there was a relatively rapid dose-dependent decrease in chromosome alignment and spindle bipolarity, which seemed to peak around 1 hour after dosing at the 30 mg/kg dose. At this dose, there was a sharp reduction in both chromosome alignment and bipolarity throughout the first 4 hours (Fig. 2C and D). At 4 hours postdose, many of the spindles showed a monopolar phenotype, which is the most commonly reported effect of Aurora A inhibition. By 8 hours, there was a partial recovery of spindle bipolarity in this dose group, but not chromosomal alignment, and the majority of spindles in this dose group were bipolar, with misaligned chromosomes. In the 10 mg/kg dose group, there was a strong reduction in chromosome alignment and spindle bipolarity in the first 4 hours (Fig 2C and D), followed by partial recovery of chromosome alignment and spindle bipolarity by 8 hours. The effects observed in the 3 mg/kg dose group were more modest, with a partial reduction of chromosomal alignment and bipolarity at 4 hours, followed by substantial recovery in chromosomal alignment by 8 hours. Taken together, alisertib at all 3 doses exhibited phenotypes that were consistent with Aurora A inhibition.

Alisertib causes tumor growth inhibition in solid tumor xenograft models and regressions in *in vivo* models of lymphoma

To determine the *in vivo* antitumor activity of alisertib, mice bearing solid and hematologic human tumor xenografts were administered increasing doses of alisertib. Figure 3A shows average tumor volumes in nude mice bearing subcutaneous HCT-116 tumors after 3 weeks of oral alisertib at 3, 10, or 30 mg/kg once daily. Alisertib treatment resulted in a dose-dependent TGI of 43.3%, 84.2%, and 94.7% for the 3, 10, and 30 mg/kg groups, respectively. The greatest antitumor response in this model was tumor stasis. All doses were well tolerated with the maximum body weight loss of 7.4% in the 30 mg/kg group.

As shown in Figure 3B, alisertib treatment in the non-Hodgkin's lymphoma model OCI-LY19 also resulted in tumor regression. Rituximab was used as a control for this model and resulted in moderate antitumor activity when dosed at 10 mg/kg once per week. Alisertib dosed at either 20 mg/kg twice daily or 30 mg/kg once daily resulted in a reduction in luminescent signal below baseline and a TGI of 106% for both groups. Moreover, tumors in the 20 mg/kg dose group did not grow back after more than 60 days of monitoring. Finally, alisertib showed broad antitumor activity across a diverse set of xenograft models, with TGI of greater than 76% at 30 mg/kg in all models tested (Table 3).

Published OnlineFirst October 20, 2011; DOI: 10.1158/1078-0432.CCR-11-1536

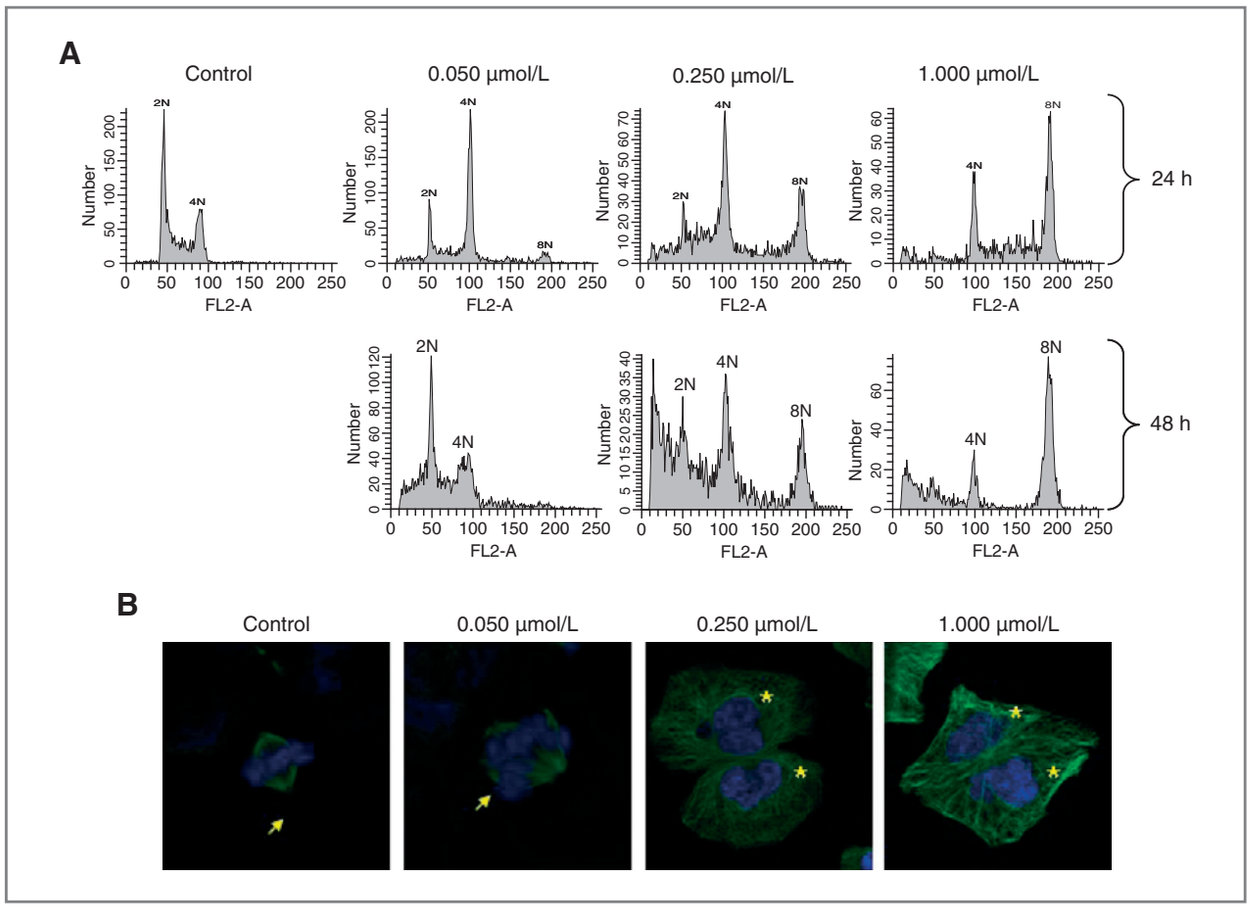

Figure 1. *In vitro* cell-based phenotypes consistent with Aurora A and Aurora B inhibition at low and high concentrations, respectively. A, flow cytometric DNA profiles of HCT-116 cells treated with DMSO or alisertib for 24 or 48 hours. Peaks 2N, 4N, and 8N reflect relative DNA content and represent diploid, tetraploid, and multinucleated cells, respectively. B, representative immunofluorescent images of HCT-116 cells treated with DMSO or alisertib (0.050, 0.250, and 1.000 μmol/L) for 24 hours. Overlapped images were obtained from cells stained with anti–α-tubulin mouse antibody (tubulin, green) and Hoechst (DNA, blue). Arrows indicate mitotic spindles and asterisks indicate multinucleated cells.

Alisertib reduces FLT uptake in HCT-116 xenograft tumors

We have shown that a dose of 20 mg/kg twice daily alisertib causes tumor stasis in the HCT-116 model, as measured volumetrically. We hypothesized that treated tumors with no change in tumor volume had a decrease in proliferating cells. Therefore, we monitored tumor response to alisertib using volumetric measurements or FLT uptake (as measured by SUV_{VOI}) using PET imaging, to determine whether noninvasive imaging of cell proliferation (as measured by FLT uptake) could be used to monitor alisertib activity and test our hypothesis. Similar to the previous study, Fig. 4A shows that alisertib inhibits tumor volume growth when compared with vehicle controls, but it does not result in tumor regressions. The difference between alisertib and vehicle groups was statistically different on days 14 and day 21 of treatment, but not on day 7. Although tumor volumes of alisertib-treated mice did not change over the course of treatment, FLT uptake and, therefore, cell proliferation, significantly decreased, starting with the first measurement on day 7, as shown in Fig. 4B. By day 21, FLT uptake in the alisertib-treated tumors decreased by 51%, which was highly statistically significant ($P = 0.0014$ by 2-tailed t test, unequal variances). As expected, the FLT uptake in tumors of the vehicle control animals did not change over the course of treatment. These results show that FLT-PET imaging may provide additional value for monitoring therapeutic response beyond volumetric measurements.

Discussion

Here we describe an orally active selective Aurora A small-molecule inhibitor that is currently in clinical development. Alisertib showed selectivity for Aurora A over Aurora B in enzyme and cell based assays, and in *in vivo* pharmacodynamic studies. At the MTD of 30 mg/kg on a daily dosing schedule, alisertib showed an increase in the mitotic index and remained pHisH3 immunopositive, a direct substrate of Aurora B. This shows that although alisertib has the ability to inhibit Aurora B at higher concentrations in cells, it does not inhibit this kinase when dosed *in vivo* at the MTD.

Published OnlineFirst October 20, 2011; DOI: 10.1158/1078-0432.CCR-11-1536

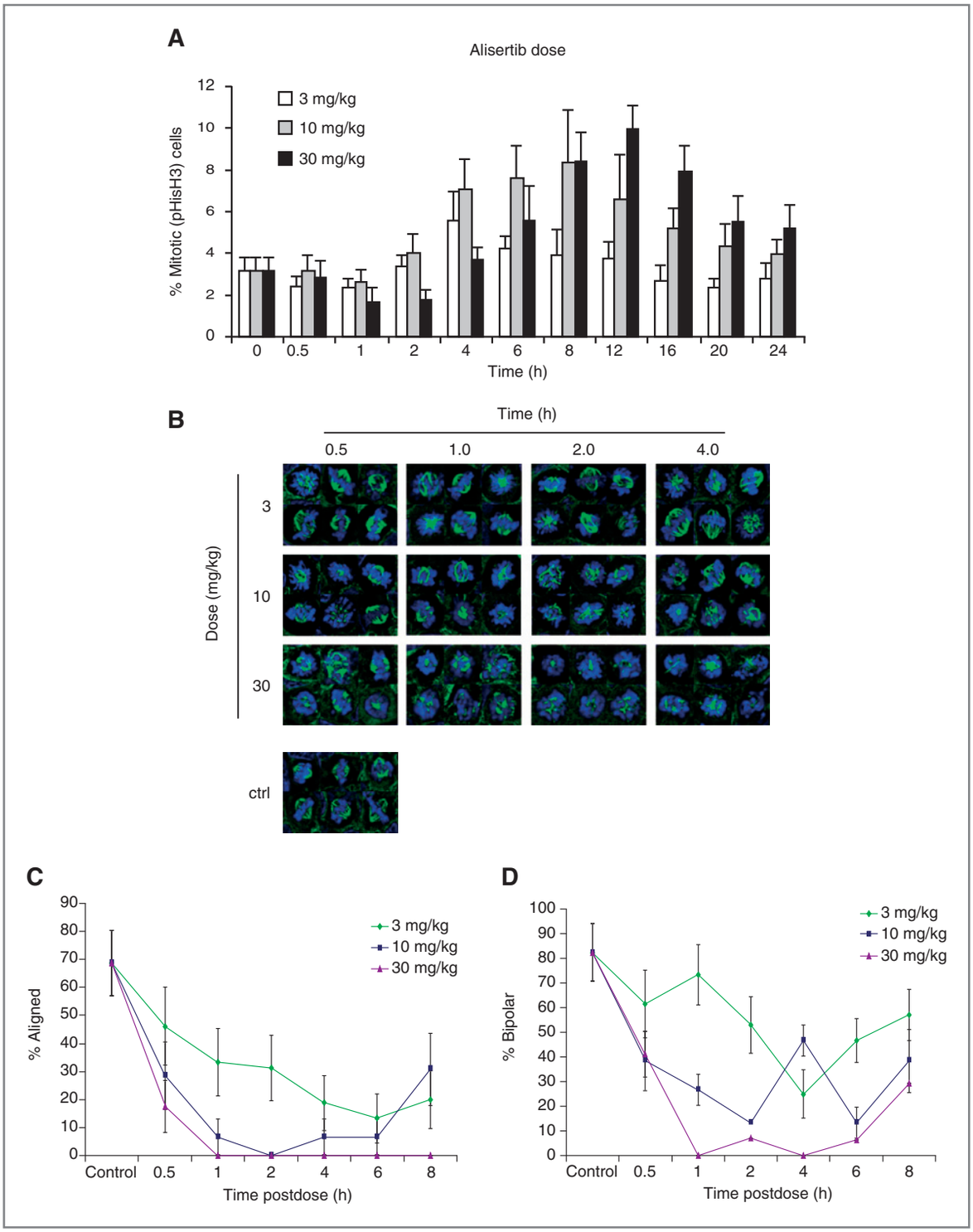

Figure 2. Pharmacodynamic activity of alisertib in the HCT-116 xenograft model as determined by increased mitotic index, misaligned chromosomes, and reduced bipolar mitotic spindles. HCT-116 tumors were treated orally with a single dose of 3, 10, and 30 mg/kg alisertib and were removed at the time points shown. A, change in mitotic index, as indicated by the mitotic marker pHisH3, following a single dose of alisertib at increasing concentrations. Tumors were stained for the mitotic marker pHisH3 using immunofluorescence detection and quantified at the indicated time points following a single dose. B, representative examples of mitotic cells taken over the first 4 hours post-alisertib. Mitotic spindles (green) were stained for α-tubulin, whereas DNA (blue) was stained with DAPI. Representative spindles are shown from each time point, showing a broad dose- and time-dependent decrease in the degree of chromosome alignment and spindle bipolarity during mitosis, consistent with the described mechanism of Aurora A. C, percentage of aligned mitotic spindles at each alisertib dose over 8 hours, as quantified by blinded, randomized visual scoring at each of the indicated time points. D, percentage of bipolar mitotic spindles at each alisertib dose above 8 hours, as similarly quantified by blinded, randomized visual scoring. Both measures show a relatively rapid dose-dependent decrease that seems to peak around 1 hour postdosing (at the highest dose).

Published OnlineFirst October 20, 2011; DOI: 10.1158/1078-0432.CCR-11-1536

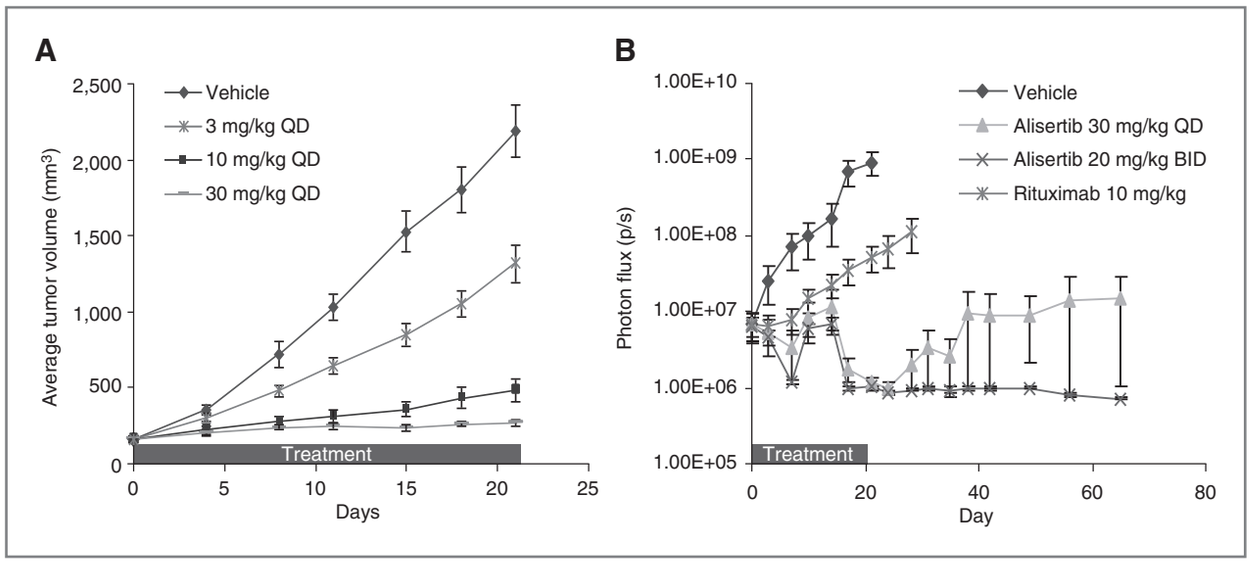

Figure 3. Broad antitumor activity of alisertib in a diverse set of human tumor xenograft models. A, nude mice bearing subcutaneous HCT-116 tumors were dosed with alisertib orally at 3, 10, and 30 mg/kg once daily for 21 consecutive days. Mean tumor volumes (mm^3) ± SEM ($n = 10$ per group) are shown from the beginning of treatment. B, OCI-LY19 tumors inoculated intravenously were treated with alisertib at 20 mg/kg twice daily, 30 mg/kg once daily, and with rituximab at 10 mg/kg once per week. Tumor burden was measured using bioluminescent imaging and expressed as whole-body photon flux ± SEM ($n = 10$ per group). BID, twice daily; QD, once daily.

The selectivity of alisertib for Aurora A relative to Aurora B was also shown in 2 human phase 1 clinical trials at the MTD, when given once daily or twice daily for 7 days, as alisertib treatment results in an increase in pHisH3 staining in both skin and tumor biopsies (44). These data show that at *in vivo* efficacious exposures, alisertib is a functionally selective inhibitor of AAK. *In vitro* immunofluorescent studies, however, indicated that at higher alisertib concentrations, cells show phenotypes consistent with Aurora B inhibition. Yang and colleagues (45) showed that the

Table 3. Alisertib antitumor activity across 9 tumor models of different histologies grown subcutaneously or disseminated

	Tumor growth inhibition (%)					
	QD dosing (mg/kg)			BID dosing (mg/kg)		
	3	10	30	3	10	20
Colon						
HCT-116	48	81	93	70	101	104
DLD-1	ND	ND	67	ND	59	96
Lung						
Calu-6	ND	−11	30	ND	ND	97
H460	21	43	91	ND	ND	ND
Prostate						
CWR22	ND	50	87	40	85	ND
Breast						
MDA-MB-231	ND	ND	63	ND	59	76
Lymphoma						
OCI-Ly7	ND	90	105	ND	106	ND
OCI-Ly19	89	104	106	ND	ND	106
WSU	51	92	ND	ND	102	108

NOTE: Mice for all models were dosed orally with alisertib for approximately 3 weeks and percent tumor growth inhibition was calculated on the last day of treatment.
Abbreviation: ND, not done.

Published OnlineFirst October 20, 2011; DOI: 10.1158/1078-0432.CCR-11-1536

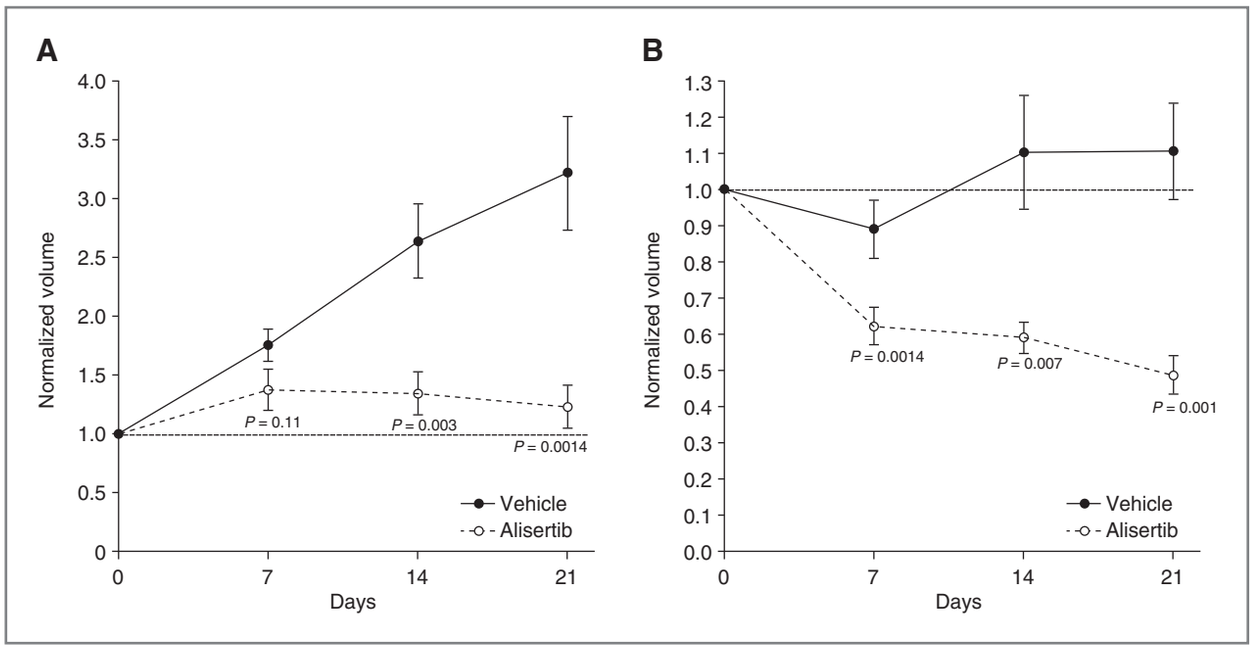

Figure 4. Alisertib reduces FLT uptake in HCT-116 tumors. HCT-116 tumors ($n = 8$ per group) were treated with alisertib at 20 mg/kg twice daily for 21 consecutive days. Mice bearing the tumors were injected with F^{18}-FLT on days 0 (pretreatment), 7, 14, and 21 and imaged using positron emission tomography (PET). A, normalized tumor volume of vehicle- and alisertib-treated mice using PET imaging. B, FLT uptake in vehicle control tumor and alisertib treated tumors using normalized SUVvol as described in the Methods.

phenotypes consistent with Aurora B inhibition are dominant over those consistent with Aurora A when both kinases are inhibited. Taken together, these data show a selectivity window of alisertib for AAK over ABK in enzyme and cell-based assays.

We used novel *in vivo* assays assessing quantitative spindle bipolarity and chromosome alignment to monitor Aurora A activity *in vivo*. These assays showed that at the MTD in mice, alisertib treatment reduced spindle bipolarity and increased chromosome misalignment. Our findings indicate that by 8 hours, spindle bipolarity, but not chromosomal alignment, had partially recovered in the 30 mg/kg dose group and that the majority of spindles in this dose group were bipolar, with misaligned chromosomes. These results are consistent with the findings reported by us as well as others in cell culture (7, 33, 41, 46) and suggests that Aurora A inhibition leads to transient mitotic arrest, followed by inappropriate passage through anaphase in the presence of misaligned chromosomes.

The transient nature and slow onset of the mitotic delays that occur with Aurora A inhibition led us to investigate these alternative mechanism-based pharmacodynamic biomarkers with a more rapid onset than the mitotic index. It is interesting to note that there is a substantial difference in time between peak mitotic index (8 to 12 hours; Fig. 2A) compared with the peak changes in the chromosome alignment and spindle bipolarity assays (1 hour; Fig. 2C and D). One potential explanation for this is that the mitotic index assay, which measures the fraction of mitotic cells in the entire population, requires several hours to accumulate mitotic cells, whereas the spindle bipolarity/chromosomal alignment assays focus on cells that are currently in mitosis, where the loss of mitotic spindle integrity upon Aurora A inhibition is rapid. An alternative explanation for the difference in kinetics between the mitotic index and the spindle bipolarity/chromosome alignment assays is the previously described role for Aurora A in mitotic commitment. Such a reduction in the rate of mitotic entry would be consistent with the delayed increase in the mitotic index observed with Aurora A inhibition.

Aurora A inhibition results in a delayed mitosis followed by an abnormal cellular division. One commonly reported outcome of Aurora A inhibition is a postmitotic p53-dependent G_1 arrest (47) that in some cases has been shown to lead to apoptosis. Cellular senescence has also been shown to be a long-term effect of Aurora A inhibition *in vitro* and *in vivo* (8).

Using markers of S-phase, BrdU, which gets incorporated into DNA, and FLT, which is phosphorylated and trapped in cells by the S-phase active thymidine kinase 1, we detected an inhibition of proliferation *in vitro* and *in vivo*. In both cases, alisertib reduced the number of cells in S phase. This could be due to transient mitotic delay, consistent with a pharmacodynamic effect of Aurora A inhibition, or due to cells undergoing apoptosis or cellular senescence. Inhibition of proliferation by Aurora A inhibition has been shown to be mediated by 2 known terminal outcomes, including apoptosis and cellular senescence (8, 32). For the *in vivo* study, there was an initial decrease in FLT uptake followed by a gradual decline to day 21. We have previously shown

Published OnlineFirst October 20, 2011; DOI: 10.1158/1078-0432.CCR-11-1536

with MLN8054, another Aurora A inhibitor similar to alisertib, that cells continue to divide for several divisions over the first few days following Aurora A inhibition (7) and undergo apoptosis as well as cell-cycle arrest during this period. This suggests that the initial decrease in FLT may not be due to senescence but, rather, apoptosis or the initial activation of the p53-dependent G_1 arrest. However, at later time points, the decrease in FLT may be due to cellular senescence, as we have previously shown; senescence, as detected by beta galactosidase staining, does not set in until day 15 and is maximal at day 21 (8).

Taken together, our data show that alisertib is a selective and potent inhibitor of AAK. In addition, we have developed novel pharmacodynamic assays to assess Aurora A target inhibition in the clinic. To this end, the spindle bipolarity and chromosome alignment assays are currently being deployed on patient skin and tumor biopsies in phase I clinical trials. These data also suggest that FLT-PET may be a valid noninvasive modality to understand multiple mechanisms of Aurora A inhibition, including cellular senescence.

Disclosure of Potential Conflicts of Interest

All authors are employees of Millennium Pharmaceuticals Inc. Josep Tabernero, Senior Editor of *Clinical Cancer Research*, is selected to conduct review process of this article. Also, Robert Wilkinson, AstraZeneca Pharmaceuticals, Macclesfield, Cheshire, United Kingdom, and Michael Henry, Office: 6-510 Bowen Science Building, Lab: 6-509 Bowen Science Building, are suggested reviewers for this article.

Acknowledgments

The authors thank Catherine Crookes of FireKite for editing assistance in the development of the manuscript, which was funded by Millennium Pharmaceuticals, Inc.

Grant Support

The work was funded by Millennium Pharmaceuticals, Inc.
The costs of publication of this article were defrayed in part by the payment of page charges. This article must therefore be hereby marked *advertisement* in accordance with 18 U.S.C. Section 1734 solely to indicate this fact.

Received June 21, 2011; revised September 11, 2011; accepted October 11, 2011; published OnlineFirst October 20, 2011.

References

1. Rovini A, Carre M, Bordet T, Pruss RM, Braguer D. Olesoxime prevents microtubule-targeting drug neurotoxicity: selective preservation of EB comets in differentiated neuronal cells. Biochem Pharmacol 2010; 80:884–94.
2. Rieder CL, Maiato H. Stuck in division or passing through: what happens when cells cannot satisfy the spindle assembly checkpoint. Dev Cell 2004;7:637–51.
3. Weaver BA, Cleveland DW. Decoding the links between mitosis, cancer, and chemotherapy: The mitotic checkpoint, adaptation, and cell death. Cancer Cell 2005;8:7–12.
4. Gascoigne KE, Taylor SS. Cancer cells display profound intra- and interline variation following prolonged exposure to antimitotic drugs. Cancer Cell 2008;14:111–22.
5. Orth JD, Tang Y, Shi J, Loy CT, Amendt C, Wilm C, et al. Quantitative live imaging of cancer and normal cells treated with Kinesin-5 inhibitors indicates significant differences in phenotypic responses and cell fate. Mol Cancer Ther 2008;7:3480–9.
6. Shi J, Orth JD, Mitchison T. Cell type variation in responses to antimitotic drugs that target microtubules and kinesin-5. Cancer Res 2008;68:3269–76.
7. Hoar K, Chakravarty A, Rabino C, Wysong D, Bowman D, Roy N, et al. MLN8054, a small-molecule inhibitor of Aurora A, causes spindle pole and chromosome congression defects leading to aneuploidy. Mol Cell Biol 2007;27:4513–25.
8. Huck JJ, Zhang M, McDonald A, Bowman D, Hoar KM, Stringer B, et al. MLN8054, an inhibitor of Aurora A kinase, induces senescence in human tumor cells both *in vitro* and *in vivo*. Mol Cancer Res 2010;8:373–84.
9. Klein LE, Freeze BS, Smith AB III, Horwitz SB. The microtubule stabilizing agent discodermolide is a potent inducer of accelerated cell senescence. Cell Cycle 2005;4:501–7.
10. Gan Y, Wientjes MG, Lu J, Au JL. Cytostatic and apoptotic effects of paclitaxel in human breast tumors. Cancer Chemother Pharmacol 1998;42:177–82.
11. Millenbaugh NJ, Gan Y, Au JL. Cytostatic and apoptotic effects of paclitaxel in human ovarian tumors. Pharm Res 1998;15: 122–7.
12. Honore S, Kamath K, Braguer D, Wilson L, Briand C, Jordan MA. Suppression of microtubule dynamics by discodermolide by a novel mechanism is associated with mitotic arrest and inhibition of tumor cell proliferation. Mol Cancer Ther 2003;2: 1303–11.
13. Torres K, Horwitz SB. Mechanisms of taxol-induced cell death are concentration dependent. Cancer Res 1998;58:3620–6.
14. Milross CG, Mason KA, Hunter NR, Chung WK, Peters LJ, Milas L. Relationship of mitotic arrest and apoptosis to antitumor effect of paclitaxel. J Natl Cancer Inst 1996;88:1308–14.
15. Schimming R, Mason KA, Hunter N, Weil M, Kishi K, Milas L. Lack of correlation between mitotic arrest or apoptosis and antitumor effect of docetaxel. Cancer Chemother Pharmacol 1999;43:165–72.
16. Symmans WF, Volm MD, Shapiro RL, Perkins AB, Kim AY, Demaria S, et al. Paclitaxel-induced apoptosis and mitotic arrest assessed by serial fine-needle aspiration: implications for early prediction of breast cancer response to neoadjuvant treatment. Clin Cancer Res 2000;6: 4610–7.
17. Gautschi O, Heighway J, Mack PC, Purnell PR, Lara PN Jr, Gandara DR. Aurora kinases as anticancer drug targets. Clin Cancer Res 2008;14:1639–48.
18. Lapenna S, Giordano A. Cell cycle kinases as therapeutic targets for cancer. Nat Rev Drug Discov 2009;8:547–66.
19. Ochi T, Fujiwara H, Yasukawa M. Aurora-A kinase: a novel target both for cellular immunotherapy and molecular target therapy against human leukemia. Expert Opin Ther Targets 2009;13:1399–410.
20. Barr AR, Gergely F. Aurora-A: the maker and breaker of spindle poles. J Cell Sci 2007;120:2987–96.
21. Lok W, Klein RQ, Saif MW. Aurora kinase inhibitors as anti-cancer therapy. Anticancer Drugs 2010;21:339–50.
22. Moore AS, Blagg J, Linardopoulos S, Pearson AD. Aurora kinase inhibitors: novel small molecules with promising activity in acute myeloid and Philadelphia-positive leukemias. Leukemia 2010;24: 671–8.
23. Cohen RB, Jones SF, Aggarwal C, von MM, Cheng J, Spigel DR, et al. A phase I dose-escalation study of danusertib (PHA-739358) administered as a 24-hour infusion with and without granulocyte colony-stimulating factor in a 14-day cycle in patients with advanced solid tumors. Clin Cancer Res 2009;15:6694–701.
24. Dees E, Infante J, Burris H, Astsaturov IA, Stinchcombe T, Liu H, et al. Phase I study of the investigational drug MLN8237, an Aurora A kinase (AAK) inhibitor, in patients (pts) with solid tumors [abstract]. J Clin Oncol 2010;28:3010.

Published OnlineFirst October 20, 2011; DOI: 10.1158/1078-0432.CCR-11-1536

25. Kristeleit R, Calvert H, Arkenau H, Olmos D, Adam J, Plummer ER, et al. A phase I study of AT9283, an aurora kinase inhibitor, in patients with refractory solid tumors [abstract]. J Clin Oncol 2009;27:2566.
26. Goldberg SL, Fenaux P, Craig MD, Gyan E, Lister J, Kassis J, et al. Phase 2 study of MLN8237, an investigational Aurora A kinase (AAK) inhibitor in patients with acute myelogenous leukemia (AML) or myelodysplastic syndromes (MDS). ASH Annual Meeting Abstracts 2010;116:3273.
27. Padmanabhan S, Shea TC, Vose JM, Reeder CB, Berdeja JG, McDonagh KT, et al. Phase I study of an investigational Aurora A kinase inhibitor MLN8237 in patients with advanced hematologic malignancies. Blood 2010;116:2799.
28. Otto T, Horn S, Brockmann M, Eilers U, Schuttrumpf L, Popov N, et al. Stabilization of N-Myc is a critical function of Aurora A in human neuroblastoma. Cancer Cell 2009;15:67–78.
29. Liu Q, Kaneko S, Yang L, Feldman RI, Nicosia SV, Chen J, et al. Aurora-A abrogation of p53 DNA binding and transactivation activity by phosphorylation of serine 215. J Biol Chem 2004;279:52175–82.
30. Wu L, Ma CA, Zhao Y, Jain A. Aurora B interacts with NIR-p53, leading to p53 phosphorylation in its DNA-binding domain and subsequent functional suppression. J Biol Chem 2011;286:2236–44.
31. Glover DM, Leibowitz MH, McLean DA, Parry H. Mutations in aurora prevent centrosome separation leading to the formation of monopolar spindles. Cell 1995;81:95–105.
32. Manfredi MG, Ecsedy JA, Meetze KA, Balani SK, Burenkova O, Chen W, et al. Antitumor activity of MLN8054, an orally active small-molecule inhibitor of Aurora A kinase. Proc Natl Acad Sci U S A 2007;104:4106–11.
33. Marumoto T, Honda S, Hara T, Nitta M, Hirota T, Kohmura E, et al. Aurora-A kinase maintains the fidelity of early and late mitotic events in HeLa cells. J Biol Chem 2003;278:51786–95.
34. Wysong DR, Chakravarty A, Hoar K, Ecsedy JA. The inhibition of Aurora A abrogates the mitotic delay induced by microtubule perturbing agents. Cell Cycle 2009;8:876–88.
35. Dar AA, Belkhiri A, Ecsedy J, Zaika A, El-Rifai W. Aurora kinase A inhibition leads to p73-dependent apoptosis in p53-deficient cancer cells. Cancer Res 2008;68:8998–9004.
36. Ditchfield C, Johnson VL, Tighe A, Ellston R, Haworth C, Johnson T, et al. Aurora B couples chromosome alignment with anaphase by targeting BubR1, Mad2, and Cenp-E to kinetochores. J Cell Biol 2003;161:267–80.
37. He L, Yang H, Ma Y, Pledger WJ, Cress WD, Cheng JQ. Identification of Aurora-A as a direct target of E2F3 during G_2/M cell cycle progression. J Biol Chem 2008;283:31012–20.
38. Marumoto T, Hirota T, Morisaki T, Kunitoku N, Zhang D, Ichikawa Y, et al. Roles of aurora-A kinase in mitotic entry and G2 checkpoint in mammalian cells. Genes Cells 2002;7:1173–82.
39. Ouchi M, Fujiuchi N, Sasai K, Katayama H, Minamishima YA, Ongusaha PP, et al. BRCA1 phosphorylation by Aurora-A in the regulation of G2 to M transition. J Biol Chem 2004;279:19643–8.
40. Prigent C, Giet R. Aurora A and mitotic commitment. Cell 2003;114:531–2.
41. Chakravarty A, Shinde V, Tabernero J, Cervantes A, Cohen RB, Dees EC, et al. Phase I assessment of new mechanism-based pharmacodynamic biomarkers for MLN8054, a small-molecule inhibitor of Aurora A kinase. Cancer Res 2011;71:675–85.
42. Shields AF, Grierson JR, Dohmen BM, Machulla HJ, Stayanoff JC, Lawhorn-Crews JM, et al. Imaging proliferation *in vivo* with [F-18]FLT and positron emission tomography. Nat Med 1998;4:1334–6.
43. Loening AM, Gambhir SS. AMIDE: a free software tool for multimodality medical image analysis. Mol Imaging 2003;2:131–7.
44. Cervantes-Ruiperez A, Burris H, Cohen R, Dees EC, Infante JR, Fingert HJ, et al. Pharmacokinetic (PK) and pharmacodynamic (PD) results from two phase I studies of the investigational selective Aurora A kinase (AAK) inhibitor MLN8237: Exposure-dependent AAK inhibition in human tumors [abstract]. J Clin Oncol 2010;28:3031.
45. Yang H, Burke T, Dempsey J, Diaz B, Collins E, Toth J, et al. Mitotic requirement for aurora A kinase is bypassed in the absence of aurora B kinase. FEBS Lett 2005;579:3385–91.
46. Sasai K, Parant JM, Brandt ME, Carter J, Adams HP, Stass SA, et al. Targeted disruption of Aurora A causes abnormal mitotic spindle assembly, chromosome misalignment and embryonic lethality. Oncogene 2008;27:4122–7.
47. Gorgun G, Calabrese E, Hideshima T, Ecsedy J, Perrone G, Mani M, et al. A novel Aurora-A kinase inhibitor MLN8237 induces cytotoxicity and cell-cycle arrest in multiple myeloma. Blood 2010;115:5202–13.

Published OnlineFirst October 20, 2011; DOI: 10.1158/1078-0432.CCR-11-1536

Clinical Cancer Research

Characterization of Alisertib (MLN8237), an Investigational Small-Molecule Inhibitor of Aurora A Kinase Using Novel *In Vivo* Pharmacodynamic Assays

Mark G. Manfredi, Jeffrey A. Ecsedy, Arijit Chakravarty, et al.

Clin Cancer Res 2011;17:7614-7624. Published OnlineFirst October 20, 2011.